NH4V3O8 Rectangular Nanotube: A Novel High-Performance Cathode Material for Lithium Ion Batteries

Lingjiang Kou (koulingjiang_sust@qq.com)
Shaanxi University of Technology https://orcid.org/0000-0001-8539-3453
Jiajia Song
Shaanxi University of Technology

Regular papers

Keywords: NH4V3O8, rectangular nanotube, electrochemical performance, cathode material, lithium ion battery

Posted Date: January 29th, 2021

DOI: https://doi.org/10.21203/rs.3.rs-160608/v1

Version of Record: A version of this preprint was published at Applied Physics A on February 11th, 2021.
See the published version at https://doi.org/10.1007/s00339-021-04325-y.

Abstract

The morphology and nanosize of cathode materials play a crucial role in the improved electrochemical properties of the electrode material for lithium ion batteries. Herein, we report the synthesis of a novel $NH_4V_3O_8$ rectangular nanotube via a facile one-pot solvothermal protocol with the use of the mixing solvent containing glycerol, ethanol, and ethylene glycol. The morphology and nanosize evolution of the as-prepared $NH_4V_3O_8$ materials from the addition of different solvents has been systematically investigated. The electrochemical properties of these materials are closely related to their structure. Compared with other synthesized counterparts with three different morphologies (nanoparticle, ultra-small nanoparticle, and hierarchical microsheet), the resultant $NH_4V_3O_8$ rectangular nanotube exhibited high reversible capacity with a maximum discharge capacity of 253.8 mAh g^{-1}at 15 mA g^{-1}, and the capacity retention rate is 75 % after 50 cycles. This work reveals the relationship between the morphology and electrochemical performance of $NH_4V_3O_8$ and provides a feasible method for the synthesis of high-performance electrode materials.

1. Introduction

At present, the application of lithium ion batteries has changed from the traditional electronic field to the new energy storage devices[1]. The performance of the battery requirements continues to increase[2, 3]. To improve energy density and power density, many researchers have made contributions[4, 5]. Extensive research on the study of lithium ion battery anodes with many studies on the application of nanomaterials such as traditional carbon materials[6–9], silicon carbon nanocomposite[10–13], alloy materials[14, 15], transition metal oxide[16, 17]. To develop a better battery and adapt to the fast-developing anode, the cathode material also needs complementary development. The cathode materials for lithium ion batteries with high energy density, high power density, high safety performance, and long cycle life are the focal point of current energy storage materials[18].

China has abundant vanadium resources and is one of the largest vanadium oxide producers in the world[19]. Vanadium derivatives and oxides have a unique layered crystal structure and good Li-ion storage performance, so they are one of the potentially high-energy and cost-effective cathode materials for Lithium Ion Batteries (LIBs)[20, 21]. For example, a versatile oxygen-deficient NaV_6O_{15} and LiV_3O_8 nanosheets display remarkable capacity properties at various current densities and excellent lithium-ion storage stability[22, 23]. The 2D nanostructured V_2O_5 exhibits enhanced lithium storage properties including high reversible capacity, good cycling, and rate performance[24, 25]. Recently, the monoclinic systems $NH_4V_3O_8$ are receiving considerable attention as alternative cathode material due to their remarkable features such as larger interlayer spacing, rapid migration of Li^+, and the network of N-H···O hydrogen bonds which increase the stability of $NH_4V_3O_8$ structure.

The electrochemical performance of electrode materials for lithium ion batteries and supercapacitors is largely dependent on their nanostructures[26–29]. Until now, there are several main methods to improve

the electrochemical performance of cathode materials. Such as surface coating by carbon material or other high conductivity material, doping, and structural control[30]. The structural control method was demonstrated to affect the materials' physical and electrochemical performance. To improve the electrochemical performance, various nanostructures of $NH_4V_3O_8$ such as nanosheets[31, 32], nanoflowers[33], nanorods[34], and nanobelts[35–37] have been synthesized. However, through continuous exploration by material researchers, the $NH_4V_3O_8$ with a novel structure can be synthesized.

In this work, the morphology and nanosize evolution on the as-prepared $NH_4V_3O_8$ materials from the addition of different solvents has been systematically investigated. The process is environmentally friendly and economically beneficial. The material morphology is controlled by adjusting the ratio of glycerol, glycol, and ethanol. By adjusting the types of solvents, different morphologies of $NH_4V_3O_8$ were synthesized, including nanoparticle (NP), ultra-small nanoparticle (SNP), rectangular nanotube (RNT), and hierarchical microsheet (HMS). Among these structures, the RNT as the cathode material of lithium ion batteries has the best electrochemical performance. The RNT delivered the discharge capacity of 253.8 mAh g^{-1}at 15 mA g^{-1}, and 75.6 % capacity retention after 50 cycles. Compared with other samples, the cycle stability of the battery has been greatly improved.

2. Experimental

All reagents and solvents were analytical grade and purchased from commercial suppliers.

2.1 Synthesis

The $NH_4V_3O_8$ nanopowders were prepared via a facile one-pot solvothermal protocol. In a typical experiment, 0.7 g ammonium metavanadate (NH_4VO_3) (purchased from Dezhou Fukai Chemical Co., Ltd) powder was added to a mixed organic solvent containing glycerol (Sinopharm Chemical Reagent Co., Ltd), ethanol (Fuyu Fine Chemical Co., Ltd) and glycol (Sinopharm Chemical Reagent Co., Ltd) either in a volume ratio of 1:2:1. The total volume of the solvent is 80 mL. Keep the filling ratio is 80 %. Heat the solution to 30 ℃ and being stirred for 1 h. After that, a proper amount of hydrochloric acid (1 mol L^{-1}) (Tianjin Bodi Chemical Co., Ltd) was further added dropwise into the above solution under continuous stirring. Finally, the resulting mixing solution was transferred into a 100 mL Teflon-lined stainless autoclave. The autoclave was sealed and heated at 160 ℃ for 12 h. After the solvothermal treatment, the autoclave was cooled down to room temperature and the precipitates were collected by vacuum filtration, then washed with deionized water and ethanol three times. The final sample was obtained after drying at 80 ℃ overnight. Then the $NH_4V_3O_8$ sample NP was obtained. For comparison, the $NH_4V_3O_8$ SNP was prepared by the above method without adding glycerol solvent, maintain the volume ratio ethanol: glycol = 2:1. $NH_4V_3O_8$ RNT was prepared through the ratio of ethanol to glycol is 1:1. Preparation of $NH_4V_3O_8$ HMS, the solvent was only ethanol.

2.2 Structure characterization

Powder X-Ray diffraction (XRD) patterns were recorded on a Rigaku D/max 2200PC V diffractometer operating with Cu Kα radiation (λ = 1.5406 Å) to characterize the crystal structure of as-prepared products. The morphology was investigated by field emission scanning electron microscopy (FESEM, S-4800, Hitachi, Japan).

2.3 Electrochemical characterization

To prepare the working electrode, the active material was mixed with sodium carboxymethyl cellulose (CMC) binder and super P together at a weight ratio of 8:1:1 in N-methyl pyrrolidone and pasted on aluminum foil. Then it was dried in a vacuum oven at 80 °C for 24 h and punched into small disks with a diameter of 15.8 mm. Electrochemical measurements were performed using CR2032 half cells, which were assembled in an argon-filled glove box (Mbraun, Germany, O_2, and H_2O contents < 0.5 ppm). Pure Li foil was used as the counter electrode and microporous polypropylene film as the separator. The electrolyte was a solution containing 1M $LiPF_6$ dissolved in a mixture of ethylene carbonate (EC), ethyl methyl carbonate (EMC), and dimethyl carbonate (DMC) (1:1:1 in volume). The galvanostatic charge/discharge tests were conducted using a Neware battery testing system with a voltage range of 1.5 to 4.0 V (vs. Li/Li^+). The other electrochemical characterizations (cyclic voltammetry and electrochemical impedance spectroscopy) were conducted using a CHI 660E electrochemistry workstation.

3. Results And Discussion

The phase structures of $NH_4V_3O_8$ samples with different morphologies were analyzed by XRD. Figure 1 represents the powder XRD pattern of prepared $NH_4V_3O_8$ samples with different morphologies. From the curves, we can deduce that the diffraction peaks of the four samples can be indexed to a monoclinic crystalline $NH_4V_3O_8$ phase (JCPDS Card No. 88-1473, space group $P2_1/m$). As seen, no other phases have been detected, showing that the products with high purity. For LiV_3O_8, the higher intensity of diffraction intensity (001), the better the degree of crystallinity[31]. Notably, with the decrease of the ethanol and glycerol, the diffraction intensity (001) peak increases, suggesting a bigger crystallite size of $NH_4V_3O_8$[35]. Unfortunately, the good ordering of crystal is disadvantageous for the diffusion of Li^+ intercalation and de-intercalation.

The morphology and micro-nano structure of the $NH_4V_3O_8$ were characterized by SEM. Figure 2 shows the SEM images of the as-prepared $NH_4V_3O_8$. When glycerol, ethanol, and ethylene glycol were used as the solvent, the $NH_4V_3O_8$ showed nanoparticle morphology with an average size of ~ 150 nm (Fig. 2a, b). When the ratio of the solvent to ethanol and ethylene glycol was 2: 1, the $NH_4V_3O_8$ showed ultra-small nanoparticles morphology with an average particle size of ~ 40 nm (Fig. 2c, d). Interestingly, when the ratio of the solvent to ethanol and ethylene glycol was 1: 1, the rectangular nanotube morphology formed (Fig. 2e, f). The average size of the tube is about ~ 140 nm. After removed ethylene glycol from the solvent, there are great morphology changes of the $NH_4V_3O_8$, it changed from nanoscale order of

magnitude to hierarchical microsheet (Fig. 2g, h). From the perspective of the crystal, morphology change is because of the oriented crystal plane.

To understand the superiority of the $NH_4V_3O_8$ rectangular nanotube, the performance of the $NH_4V_3O_8$ NP, SNP, RNT, and HMS as cathodes in lithium ion battery was investigated. Figure 3 exhibits the cycling performance and rate performance of the as-prepared $NH_4V_3O_8$. The voltage range is 1.5-4.0 V (vs. Li/Li^+). The cycle performance of the electrodes is shown in Fig. 3a. After 50 cycles RNT exhibits a discharge capacity of 189.5 mAh g^{-1} at 15 mA g^{-1}, while the discharge capacity for NP, SNP, and HMS are only 157.8, 154, and 46.8 mAh g^{-1}, respectively. It shows that the RNT sample has a significantly improved lithium storage capability. We can get the Coulomb Efficiency (CE) of the sample RNT. The CE of RNT has been maintained at high levels, coincides with better cycling performance. Figure 3b shows the rate performance of the different $NH_4V_3O_8$ samples at a current density from 15 mA g^{-1} to 300 mA g^{-1}. The rate performance of RNT shows higher capacity retention than the other three samples. After 300 cycles the discharge capacity of RNT can revert to 131.1 mAh g^{-1}, while those for NP, SNP, and HMS are only 85.4, 72.1, and 40 mAh g^{-1}, respectively. The reason for the good electrochemical performance of $NH_4V_3O_8$ is the structure of rectangular nanotube which promotes the contact area between $NH_4V_3O_8$ and electrolyte, enhances the diffusion efficiency. Table 1 is the comparison of the electrochemical performance of as-prepared $NH_4V_3O_8$ and other different morphology $NH_4V_3O_8$ reported in the literature. Despite the initial discharge capacity and capacity retention of other $NH_4V_3O_8$ material is a litter better than sample RNT, the number of cycles is small. In this paper, after 50 cycles, the discharge capacity retention rate maintains 75 %.

Table 1
Comparison of the capacity and capacity retention reported in recent papers for $NH_4V_3O_8$

Morphology	Synthesis method	Initial discharge capacity	Cycle number	Capacity retention	Measured current density ($mA\ g^{-1}$)	References
Regular hexagonal micro plates	Microwave assisted hydrothermal	270	3	-	10	[38]
Flower	Microwave hydrothermal	312	20	78 %	15	[39]
Nanobelt	Microwave hydrothermal	328	20	94 %	15	[39]
Nanorods	Water-bath	208	30	104 %	15	[40]
rectangular nanotube	Solvothermal	253	50	75 %	15	This paper

The Nyquist plots of the as-prepared samples are compared in Fig. 4a. Firstly charged the battery to 4.0 V, and then measure electrochemical impedance spectroscope in the frequency range from 0.01 Hz to 100 kHz. $NH_4V_3O_8$ RNT shows a much lower charge transfer resistance is 98.4 Ω, suggesting that it is easy to transfer for Li^+ and electrons during the charge and discharge process. To better understand the plots, an equivalent circuit model was used to fit the impendence in Fig. 4a. The parameters R_e, CPE, R_{ct}, and W correspond to the Ohmic resistance of the electrolyte and electrode in the battery, constant phase element, the charge transfer resistance of corresponding electrochemical reactions, and the Warburg impedance related to Li^+ diffusion, respectively. The value of R_{ct} of different samples could be simulated from the EIS date by using the equivalent circuit. Figure 4b is the histogram of comparing each resistance value. It could be seen that the R_{ct} value for RNT, HMS, NS, and NP was 83.2, 106.1, 86.8, and 97.2, respectively. The value of the total resistance of RNT is smaller than the other three samples. The results of electrochemical impedance spectroscope measurements are in good agreement with the electrochemical performance.

The charge/discharge curves of the sample RNT at different cycles shows in Fig. 5a.The discharge capacity of $NH_4V_3O_8$ RNT at the 1st, 2nd, 10th, 25th, and 50th cycle is 269, 250, 233, 215, and 208 mAh g^{-1}, respectively. There are three discharge voltage plateaus at 2.75, 2.49, and 2.1 V, and the voltage plateaus indicate the multi-step Li^+ intercalation/de-intercalation process. Figure 5b depicts the galvanostatic voltage profile of $NH_4V_3O_8$ RNT at different specific currents. The charge capacity increase and the discharge specific capacity decrease with the variation of current densities from 15 to 300 mA g^{-1}, because of the sluggish Li^+ diffusion kinetics at high current densities[41].

To clarify the better electrochemical performance of $NH_4V_3O_8$ RNT, the CV measurement at different sweep rates was conducted. The CV analysis is performed to estimate the kinetic and mass transport during the redox process of cathode materials. Figure 6a shows the CV curves of the $NH_4V_3O_8$ RNT measured in the voltage range of 1.5-4.0 V at a scan rate of 0.1 mV s^{-1}. The $NH_4V_3O_8$ RNT shows a peak at 2.48 V and vanishes in the following cycles, corresponding to irreversible lithium insertion into $NH_4V_3O_8$ in the first two cycles. Figure 6b shows the CV curves of the $NH_4V_3O_8$ RNT measured in the voltage range of 1.5-4.0 V at different scan rates. As the scan rate increase from 0.1 to 0.8 mV s^{-1}, the shape of the redox peaks is well preserved, implying that small polarization, fast Li^+ insertion/desertion, and good reversibility of $NH_4V_3O_8$ RNT.

4. Conclusions

In summary, shape-controlled $NH_4V_3O_8$ was prepared via a facile one-pot solvothermal method. By adjusting the ratio of the solvent, the morphology of the material can be effectively adjusted. The lithium storage performance of as-prepared was through systematic research. The synthesized $NH_4V_3O_8$ RNT exhibited a high discharge capacity of 253.8 mAh g^{-1} at 15 mA g^{-1} and good cyclic stability. The excellent electrochemical performance of as-prepared $NH_4V_3O_8$ RNT is benefited from the hollow

rectangular nanotube which can provide more reactive active sites. This facile synthetic strategy is expectable to offer an interesting clue for the morphological engineering of other nano-sized electrode materials currently employed in lithium-based batteries.

The corresponding authors declare no conflict of interest. There are no interests to declare.

Declarations

The corresponding authors declare no conflict of interest. There are no interests to declare.

Acknowledgments

This work was supported by the Research Program of Shaanxi University of Technology (SLGRCQD2025) and financial support from the China Scholarship Council(201808610234).

References

1. Zhao N, Fan H, Zhang M, Wang C, Ren X, Peng H, Li H, Jiang X, Cao X, Journal of Alloys and Compounds 796:111-119. (2019)
2. Lin D, Liu Y, Cui Y, Nat Nanotechnol 12 (3):194-206. (2017)
3. Manthiram A, Yu X, Wang S, Nature Reviews Materials 2 (4):16103. (2017)
4. Zhang M, Fan H, Zhao N, Peng H, Ren X, Wang W, Li H, Chen G, Zhu Y, Jiang X, Wu P, Chemical Engineering Journal 347:291-300. (2018)
5. Ren X, Fan H, Ma J, Wang C, Zhang M, Zhao N, Applied Surface Science 441:194-203. (2018)
6. Wu YP, Rahm E, Holze R, J Power Sources 114 (2):228-236. (2003)
7. Hou H, Qiu X, Wei W, Zhang Y, Ji X, Advanced Energy Materials 7 (24):1602898. (2017)
8. Zheng Y, Wang Y, Lu Y, Hu Y-S, Li J, Nano Energy 39:489-498. (2017)
9. Yu H, Dong X, Pang Y, Wang Y, Xia Y, Electrochim Acta 228:251-258. (2017)
10. Wang Y, Wu H, Xiao FM, Tang RH, Sun T, Materials Science Forum 914:64-70. (2018)
11. Cai H, Han K, Jiang H, Wang J, Liu H, J Phys Chem Solids 109:9-17. (2017)
12. Liang Y, Liu DG, Bai WQ, Tu JP, Colloids and Surfaces B: Biointerfaces 153:41-51. (2017)
13. Ren D, Huang H, Qi J, Zheng P, Energy Technology 8 (7):2000314. (2020)
14. Xie H, Kalisvaart WP, Olsen BC, Luber EJ, Mitlin D, Buriak JM, J Mater Chem A 5 (20):9661-9670. (2017)
15. Yu L, Liu J, Xu X, Zhang L, Hu R, Liu J, Yang L, Zhu M, Acs Appl Mater Inter 9 (3):2516-2525. (2017)
16. Jiang Y, Li Y, Zhou P, Lan Z, Lu Y, Wu C, Yan M, Adv Mater 29 (48):1606499. (2017)
17. Zhu S, Li J, Deng X, He C, Liu E, He F, Shi C, Zhao N, Advanced Functional Materials 27 (9):1605017. (2017)

18. Bini M, Capsoni D, Ferrari S, Quartarone E, Mustarelli P (2015) 1 - Rechargeable lithium batteries: key scientific and technological challenges A2 - Franco, Alejandro A. In: Rechargeable Lithium Batteries. Woodhead Publishing, pp 1-17. doi:https://doi.org/10.1016/B978-1-78242-090-3.00001-8
19. Moskalyk RR, Alfantazi AM, Minerals Engineering 16 (9):793-805. (2003)
20. Wei Q, Liu J, Feng W, Sheng J, Tian X, He L, An Q, Mai L, J Mater Chem A 3 (15):8070-8075. (2015)
21. Zhang C, Park S-H, O'Brien SE, Seral-Ascaso A, Liang M, Hanlon D, Krishnan D, Crossley A, McEvoy N, Coleman JN, Nicolosi V, Nano Energy 39:151-161. (2017)
22. Song H, Luo M, Wang A, ACS Applied Materials & Interfaces 9 (3):2875-2882. (2017)
23. Wang HY, Huang KL, Ren Y, Huang XB, Liu SQ, Wang WJ, J Power Sources 196 (22):9786-9791. (2011)
24. Liang S, Hu Y, Nie Z, Huang H, Chen T, Pan A, Cao G, Nano Energy 13:58-66. (2015)
25. Lee JH, Kim J-M, Kim J-H, Jang Y-R, Kim JA, Yeon S-H, Lee S-Y, Advanced Materials Interfaces 3 (14):1600173. (2016)
26. Li X, Fu J, Pan Z, Su J, Xu J, Gao B, Peng X, Wang L, Zhang X, Chu PK, Journal of Power Sources 331:58-66. (2016)
27. Ding Y-L, Wen Y, Wu C, van Aken PA, Maier J, Yu Y, Nano Letters 15 (2):1388-1394. (2015)
28. Dong G, Fan H, Fu K, Ma L, Zhang S, Zhang M, Ma J, Wang W, Composites Part B: Engineering 162:369-377. (2019)
29. Zheng P, Su J, Wang Y, Zhou W, Song J, Su Q, Reeves-McLaren N, Guo S, ChemSusChem 13 (7):1793-1799. (2020)
30. Cao J, Guo S, Yan R, Zhang C, Guo J, Zheng P, Journal of Alloys and Compounds 741:1-6. (2018)
31. Wang H, Huang K, Liu S, Huang C, Wang W, Ren Y, Journal of Power Sources 196 (2):788-792. (2011)
32. Cao SS, Huang JF, Li JY, Xu ZW, Ouyang HB, Zheng L, Mater Lett 148:192-195. (2015)
33. Kou L, Cao L, Huang J, Yang J, Wang Y, Journal of Materials Science: Materials in Electronics 29 (6):4830-4834. (2018)
34. Wang HY, Ren Y, Wang WJ, Huang XB, Huang KL, Wang Y, Liu SQ, J Power Sources 199:315-321. (2012)
35. Kou L, Cao L, Huang J, Yang J, Micro Nano Lett. (2017)
36. Cao SS, Huang JF, Cheng YY, Li RZ, Li JY, Xu ZW, Ouyang HB, Cao LY, Wu JP, J Electroanal Chem 752:12-16. (2015)
37. Ottmann A, Zakharova GS, Ehrstein B, Klingeler R, Electrochimica Acta 174:682-687. (2015)
38. Zakharova GS, Ottmann A, Ehrstein B, Klingeler R, Materials Research Bulletin 83:225-229. (2016)
39. Cheng Y, Huang J, Li J, Cao L, Xu Z, Wu J, Cao S, Hu H, Electrochimica Acta 212:217-224. (2016)
40. Cao S-S, Huang J-F, Ouyang H-B, Cao L-Y, Li J-Y, Wu J-P, Materials Letters 126:20-23. (2014)
41. Wang X, Feng Z, Huang J, Deng W, Li X, Zhang H, Wen Z, Carbon 127:149-157. (2018)

Figures

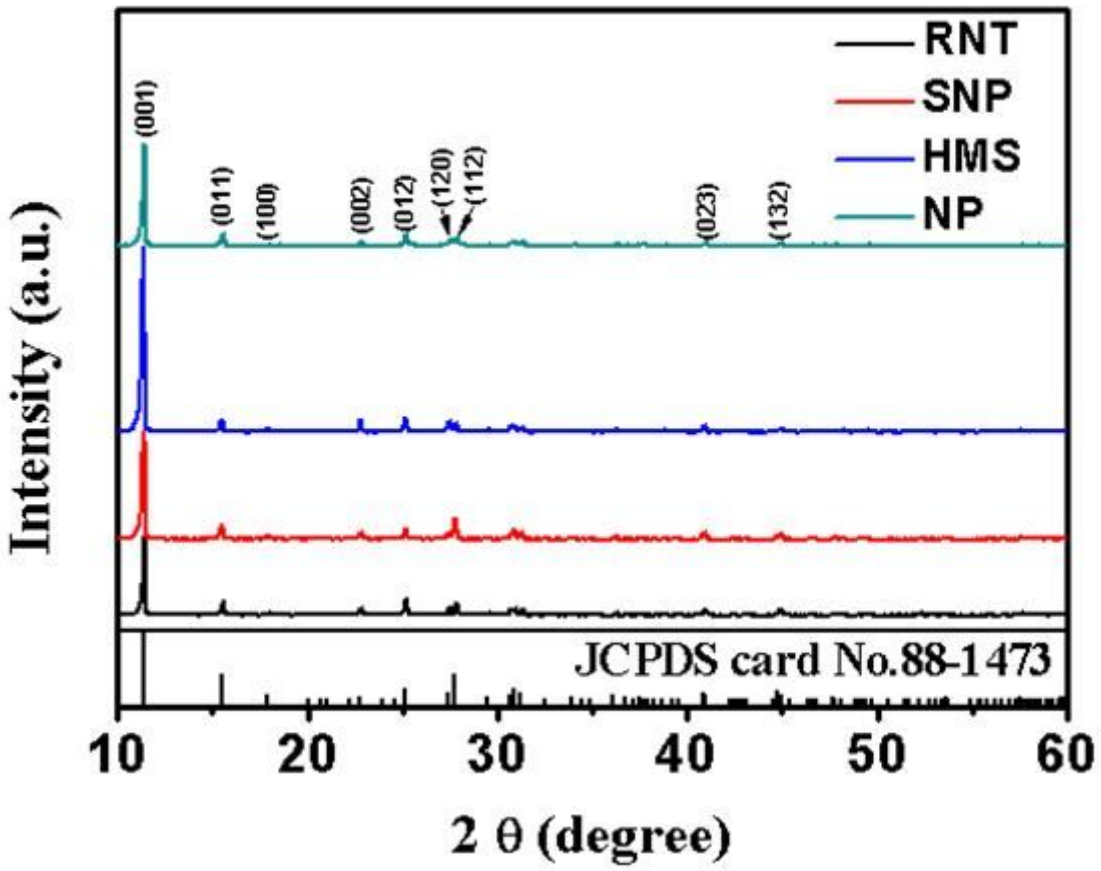

Figure 1

XRD pattern of the as-prepared NH4V3O8 samples

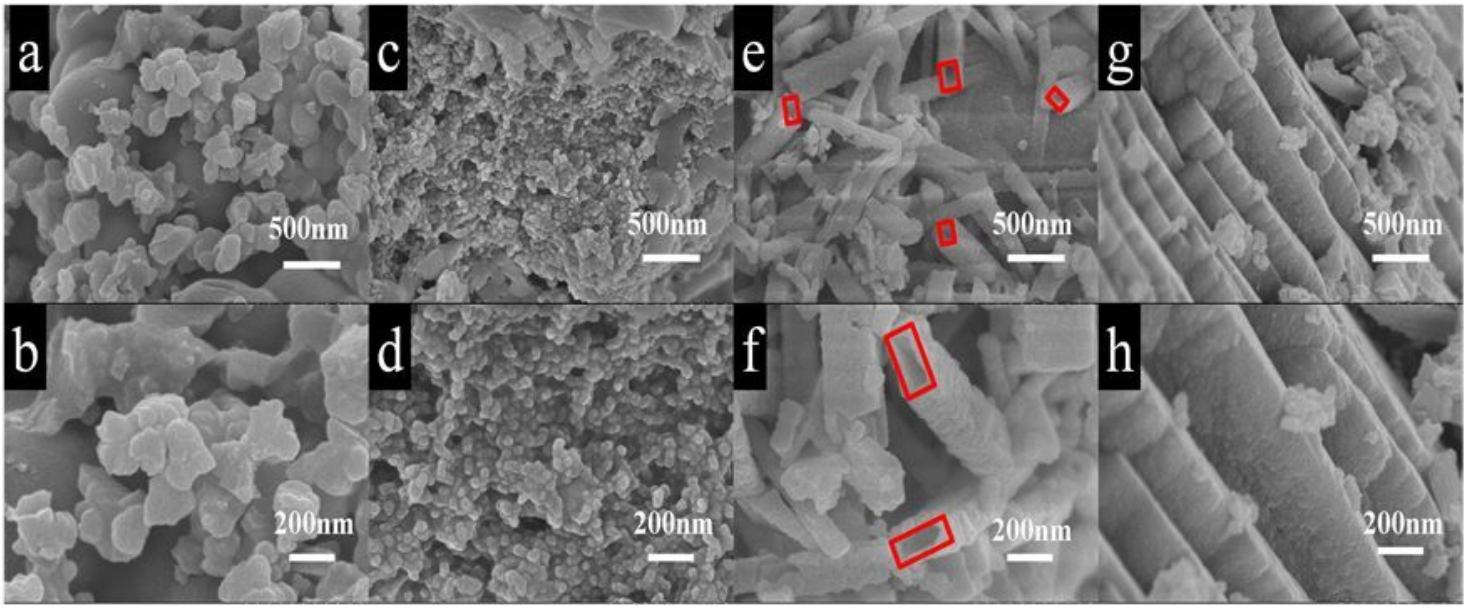

Figure 2

SEM images of as-prepared NH4V3O8 (a, b) nanoparticle (NP), (c, d) ultra-small nanoparticle (SNP), (e, f) rectangular nanotube (RNT), (g, h) hierarchical microsheet (HMS)

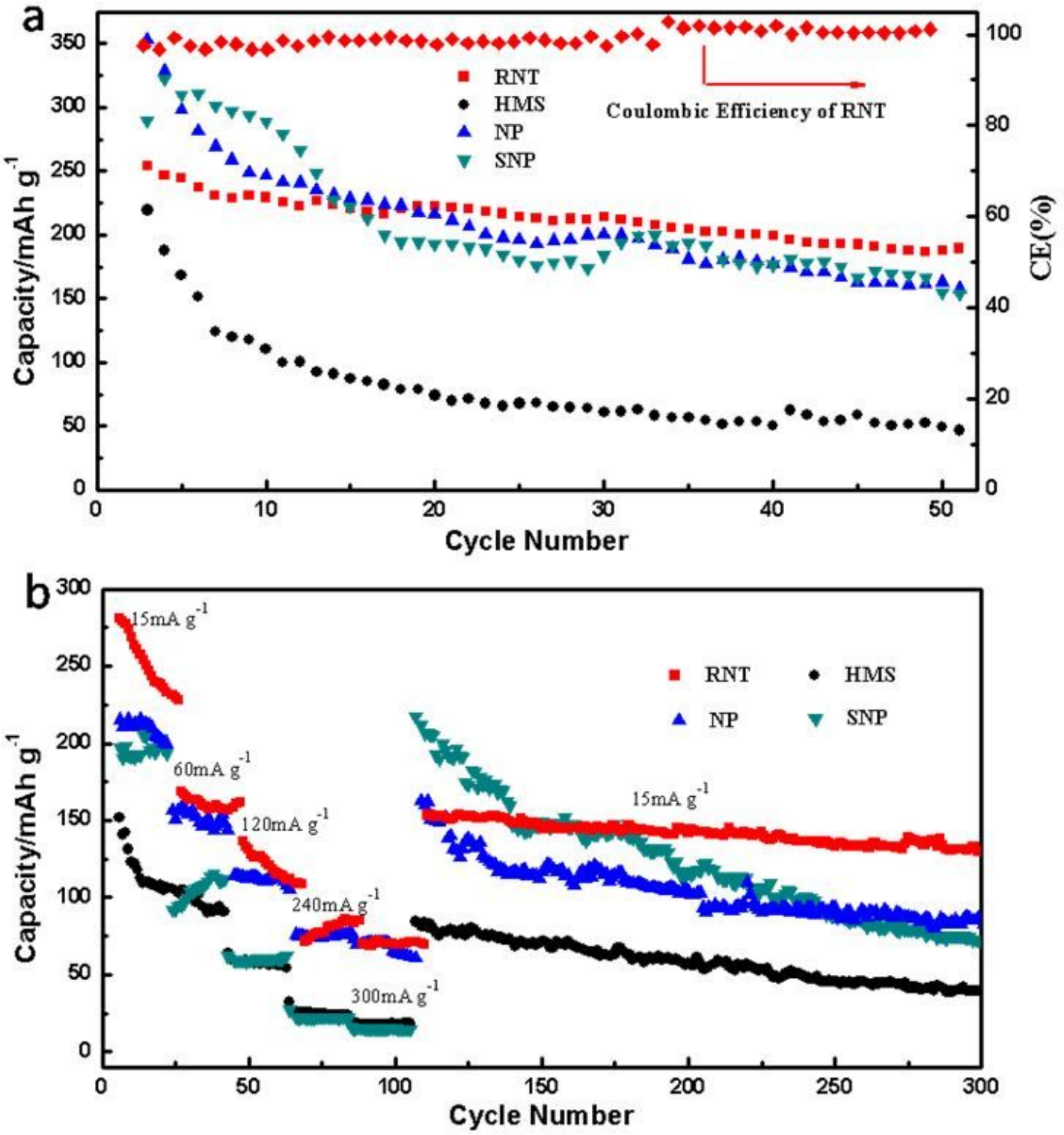

Figure 3

(a) Cycling performance and of as-prepared NH4V3O8 at a current density of 15 mA g-1; (b) Rate performance of as-prepared NH4V3O8 at different current density.

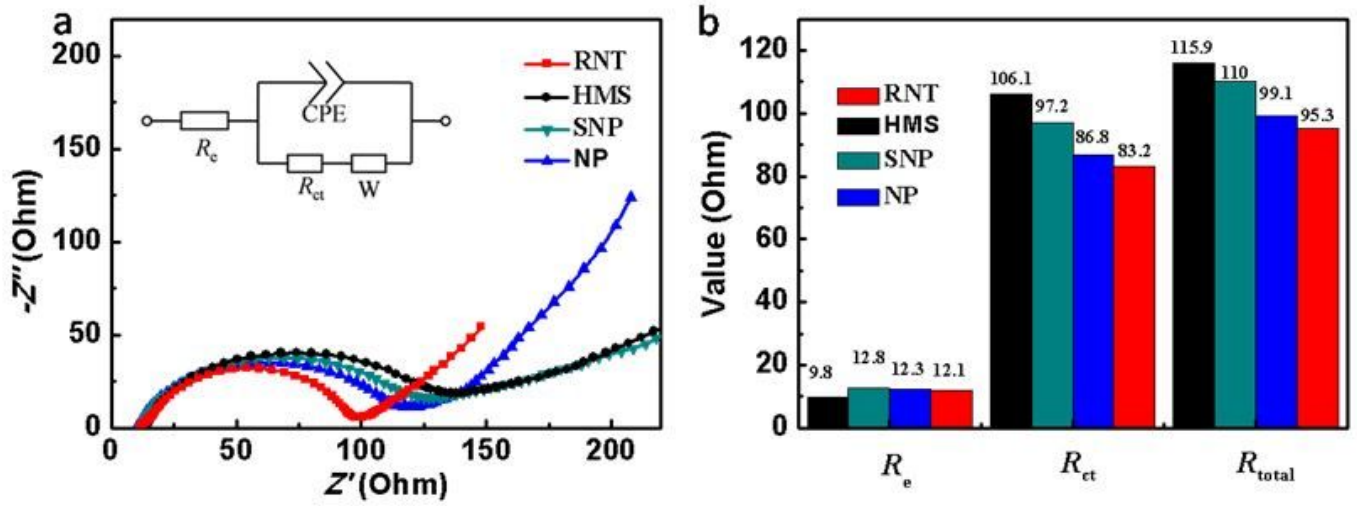

Figure 4

(a) The Nyquist plot of the NH4V3O8 electrode, inset is the equivalent circuit model used to simulate the spectra; (b) histogram of comparing each resistance value in the equivalent circuit of the four samples.

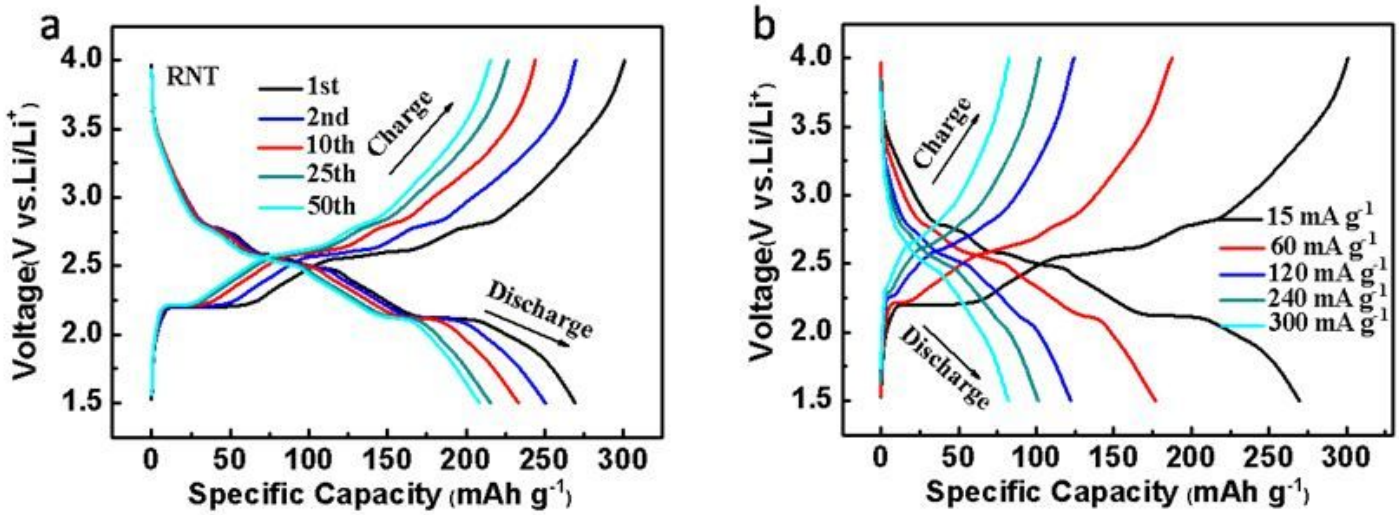

Figure 5

(a) typical charge/discharge curves of NH4V3O8 at 15 mA g-1 for RNT. (b) charge/discharge curves of RNT in the potential region from 1.5 to 4.0V at different current densities.

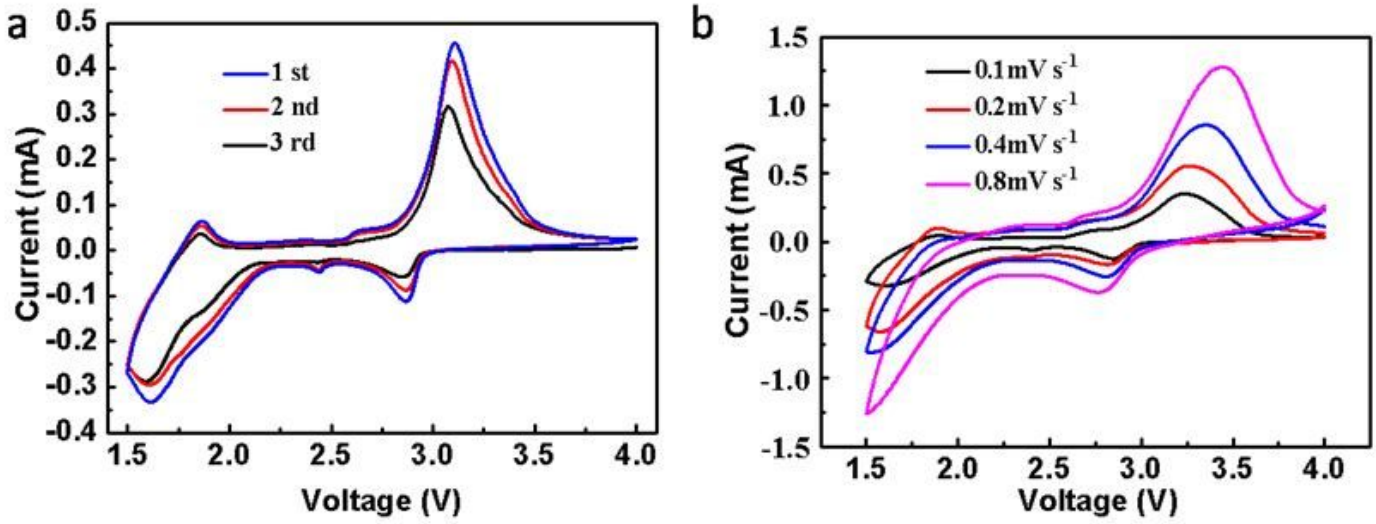

Figure 6

CV curves of the NH4V3O8 RNT were measured in the voltage range of 1.5-4.0 V. (a) at a scan rate of 0.1 mV s-1. (b) at different scan rates.